Energy & Environmental Science

Accepted Manuscript

This article can be cited before page numbers have been issued, to do this please use: X. Li, X. Wu, S. Son, J. M. Seminario, P. B. Balbuena, A. Arboleda, J. Cai, M. Li, Z. Lyu, D. Bresser, R. Amine, C. C. Su and K. Amine, *Energy Environ. Sci.*, 2025, DOI: 10.1039/D5EE01515D.

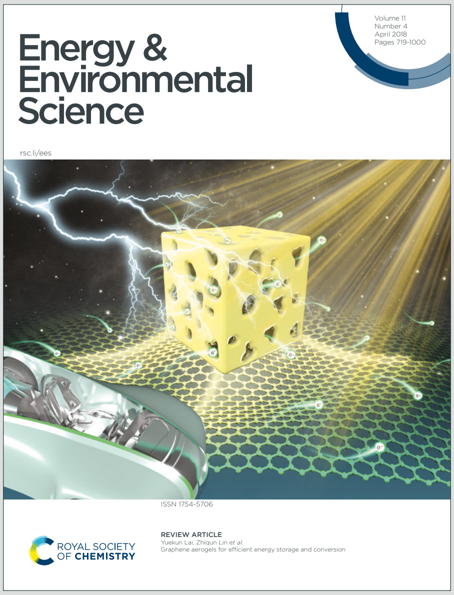

View Article Online
DOI: 10.1039/D5EE01515D

Broader context statement

Ionic liquid-based electrolytes, particularly those with Py13FSI, have gained attention for their potential to enhance the performance of lithium metal batteries (LMBs) due to their stability and non-flammability. However, a major challenge in advancing these electrolytes is achieving a stable and efficient electrolyte-cathode interface. This study highlights the role of co-solvents, specifically FDG, in optimizing the solvation environment to improve battery performance. By stabilizing the cathode interphase and promoting efficient Li^+ transport with reduced over-potential, FDG significantly extends cycling life. Our findings emphasize the importance of balancing solvation properties when designing new electrolytes, as a medium-range solvation shell is crucial for forming a stable electrolyte-cathode interface. This work provides valuable insights into the design of future electrolytes by carefully selecting co-solvents that balance solvating capabilities, offering a pathway to developing more durable and high-performance electrolyte systems.

View Article Online
DOI: 10.1039/D5EE01515D

Balancing Solvation: Stabilizing Lithium Metal Batteries via Optimized Cosolvents in Ionic-liquid Electrolytes

Xinlin Li,[a] Xianyang Wu,[a] Seoung-Bum Son,[a] Jorge Seminario,[b, d, e*] Perla Balbuena,[b, e, f*] Anderson Arboleda,[b] Jiyu Cai,[a] Matthew Li,[a] Ziyuan Lyu,[g,h] Dominic Bresser,[g,h] Rachid Amine,[c] Chi-Cheung Su,[a*] and Khalil Amine[a*]

[a] Chemical Sciences and Engineering Division, Argonne National Laboratory, 9700 S. Cass Avenue, Lemont, IL 60439, USA

[b] Department of Chemical Engineering, Texas A&M University, College Station, Texas, 77843, USA

[c] Materials Science Division, Argonne National Laboratory, 9700 S. Cass Avenue, Lemont, IL 60439, USA

[d] Department of Electrical and Computer Engineering, Texas A&M University, College Station, Texas, 77843, USA

[e] Department of Materials Science and Engineering, Texas A&M University, College Station, Texas, 77843, USA

[f] Department of Chemistry, Texas A&M University, College Station, Texas, 77843, USA

[g] Helmholtz Institute Ulm (HIU), Electrochemical Energy Storage, 89081 Ulm, Germany

[h] Karlsruhe Institute of Technology (KIT), 76021 Karlsruhe, Germany

E-mail: csu@anl.gov; seminario@tamu.edu; balbuena@tamu.edu; amine@anl.gov

Abstract

In this study, we examined three cosolvents with distinct solvation capabilities for ionic-liquid-based electrolytes, 1-methyl-1-propyl pyrrolidinium bis(fluorosulfonyl)imide (**Py13FSI**). Among them, we demonstrate that 1,1,1-trifluoro-2-(2-(2-(2,2,2-trifluoroethoxy)ethoxy)ethoxy)ethane (**FDG**), notably enhances the cycle life of Py13FSI-based electrolytes, outperforming 1,1,2,2-tetrafluoroethyl 2,2,3,3-tetrafluoropropylether (**TTE**) and diglyme (**DG**). Electrochemical and surface analyses attribute this improvement to the formation of a favorable cathode interphase, promoting efficient Li^+ transport with

View Article Online
DOI: 10.1039/D5EE01515D

reduced overpotential. Spectroscopic techniques (FTIR, Raman, and NMR spectroscopy) and molecular dynamics simulations reveal that cosolvents with varying solvation abilities influence the solvation structures in Py13FSI-based electrolytes. The mild solvating strength and lithium stability of FDG are key contributors to its effectiveness. Conversely, DG, a strong solvating solvent, destabilizes the Py13FSI-DG electrolyte at the lithium metal anode, while TTE, a non-solvating solvent, fails to enhance lithium transport or form a stable cathode interphase. Our findings highlight that a balanced solvation exerted by cosolvents is critical for forming a stable electrolyte-cathode interface, potentially through FSI decomposition. This study offers valuable insights into the development of durable ionic liquid electrolytes, emphasizing the importance of selecting cosolvents with optimal solvation properties.

Introduction

Lithium metal batteries (LMBs) represent a promising frontier in the realm of energy storage technologies, due to their exceptionally high theoretical capacity (3860 mAh g^{-1}) and very low redox potential (-3.04 V vs SHE).[1, 2] The synergistic utilization of a lithium-metal anode alongside nickel-rich cathode materials such as $LiNi_{1-x-y}Mn_xCo_yO_2$ (NMC) stands out as one of the most promising combinations in the pursuit of high-energy-density batteries.[3-5] However, the highly oxidative NMC and highly reductive lithium anode exert challenges on the robustness of electrolytes which are vulnerable to parasitic degradations at the electrolyte-electrode interfaces. The reversibility of lithium plating/stripping relies heavily on the electrochemical stability of the passivation interphases on both cathode and anode formed during cycling.[6-10] Although excellent overall cell performance has been demonstrated, state-of-the-art organic electrolytes exhibit unsatisfactory Coulombic efficiency, capacity retention, and safety concerns due to their low cathodic/anodic stability in LMBs and their high flammability.[11, 12]

Extensive efforts have been made to exploit promising electrolyte systems that can overcome the aforementioned issues in LMBs such as highly-concentrated[13-16] and localized-high-concentration electrolytes[17-20]. Across a large variety of potential solvents capable of solvating lithium ions, ionic liquids (**ILs**), a class of salts existing in the liquid state at ambient temperatures with a negligible vapor pressure,

View Article Online
DOI: 10.1039/D5EE01515D

have emerged as a compelling alternative to conventional organic solvents due to their remarkable solvation capability of Li^+ (*i.e.* typically in the form of lithium bis(fluorosulfonyl)imide, LiFSI or bis(trifluoromethylsulfonyl)imide, LiTFSI), electrochemical stability, and low flammability.[21-26] It has been studied that the broad electrochemical windows of various ILs enabling them to be promising solvents in electrochemical applications including lithium batteries.[27, 28] Despite IL electrolytes' high cycling stability in LMBs revealed by recent research, their overall cell performance is limited by the intrinsically high viscosity and sluggish Li^+ transport. Therefore, electrolyte engineering, typically the incorporation of cosolvents that modulate solvation structures and reduce the overall viscosity, which could be beneficial for interfacial stability, is regarded as a very effective approach to enhance ionic conductivity and ideally also cycling stability.[22, 29-31]

The steric hindrance of the IL cation makes it less favorable in the close solvation shell than the dissolved Li^+ with a smaller ionic radius.[32] The solvation sheath is therefore mainly comprised of Li^+ and the FSI anion in pristine IL electrolytes.[33-35] Among the reported cosolvents, the ones with strong solvating capabilities such as carbonates and ethers usually intervene Li ions' solvation with FSI anions, which is unfavorable for stable interphases in LMBs.[29, 30] Non-solvating cosolvents, such as 1,1,2,2-tetrafluoroethyl 2,2,3,3-tetrafluoropropylether (**TTE**) and bis(2,2,2-trifluoroethyl) ether (**BTFE**), which are electrochemically stable in cell environments, offer new possibilities to overcome the challenges of IL-based electrolytes. They significantly reduce the total viscosity of the IL electrolyte without participating in the straightforward solvation of the lithium complexes.[22, 29, 30] However, the addition of non-solvating solvents may alter the overall lithium solvating ability and the dielectric constant of electrolyte solvents, which further affects lithium transport.[30, 31] Thus, it is challenging to balance the cosolvents' solvation capabilities, oxidation/reduction stability, and physical properties such as viscosity and ionic conductivity (especially lithium transport capability) in IL-based electrolytes to reach the optimal cell performance.

Herein, we developed an electrolyte system comprised of the IL, 1-methyl-1-propyl pyrrolidinium bis(fluorosulfonyl)imide (**Py13FSI**), and a fluorinated diethylene glycol ether 1,1,1-trifluoro-2-(2-(2-

View Article Online
DOI: 10.1039/D5EE01515D

(2,2,2-trifluoroethoxy)ethoxy)ethoxy)ethane (**FDG**), as the optimal solvating cosolvent, which demonstrated excellent capacity retention in Li||NMC811 ($LiNi_{0.8}Mn_{0.1}Co_{0.1}O_2$) cells. To the best of our knowledge, this is the first demonstration of incorporating a glycol ether-type cosolvent into an IL-based electrolyte in LMBs. The comparison among three distinct cosolvents, i.e., diglyme (**DG**), FDG, and TTE, which have descending lithium solvating capabilities, allows for distinguishing the unique electronic and solvation properties of FDG compared to the other cosolvents in order to obtain enhanced capacity retention in LMBs. The results show that FDG, with its suitable lithium solvating ability and appropriate electrochemical stability window, serves as the optimal cosolvent for IL-based electrolytes. The Li||NMC811 cells using IL-FDG electrolyte displayed a significantly reduced over potential for Li intercalation into the NMC cathode upon long-term cycling and enhanced capacity retention compared to the other formulations. These results strongly suggest that both the electrolyte-anode and electrolyte-cathode interphases are stabilized in the IL-FDG cell, as evidenced by electrochemical and surface analysis techniques. Moreover, the beneficial effect of incorporating FDG into the electrolyte is also evident in the

View Article Online
DOI: 10.1039/D5EE01515D

stabilization of the cathode-electrolyte interphases (CEI), achieved through the alteration of the solvation sheath, as indicated by the molecular dynamics (MD) simulation results.

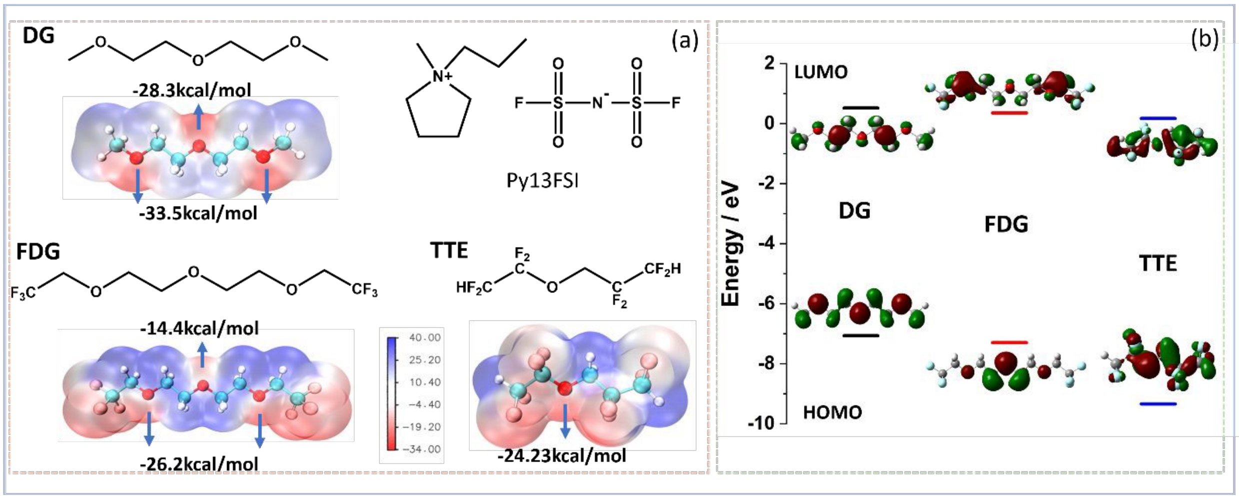

Figure 1. (a) Structures of Py13FSI and cosolvents and calculated molecular electrostatic potential (MEP) on isodensity surfaces of DG, FDG, and TTE showing negative (red) and positive (blue) regions; (b) Calculated HOMO and LUMO energies and wavefunctions of three cosolvents.

Results and Discussion

Study of solvation structures enabled by different cosolvents: The electrolytes are formulated by dissolving LiFSI (1.4m) in the liquid phase comprised of Py13FSI and the desired cosolvents in a volumetric ratio of 4:1. Three cosolvents with distinct solvating capabilities reflected by their molecular electrostatic potential (**MEP**) (**Figure 1a**) and oxidation/reduction potential (as indicated by their HOMO and LUMO energies, **Figure 1b**) are utilized in this work. Viscosity measurements (**Figures S1 and S2**) manifest the reduced viscosity upon the addition of cosolvents from 77 cP in the neat Py13FSI electrolyte to 45 and 54 cP at 20 °C in Py13FSI+TTE and Py13FSI+FDG respectively. The Solvation structures of the IL-based electrolytes were experimentally studied via Fourier Transform Infrared (FTIR) (**Figure 2a**), Raman (**Figure 2b**), and NMR spectroscopy (**Figure 2c**). The IR absorption in the 800-880 cm^{-1} range (this range was targeted due to the noninterference by cosolvents) highlights the S-N-S asymmetric stretching

View Article Online
DOI: 10.1039/D5EE01515D

from the FSI anion (**Figure 2a**). Dissolving 1.4m of LiFSI in Py13FSI results in a peak shift from 825 to 834 cm^{-1}, underscoring the sulfonyl groups' coordinating the Li$^+$ ions (**Figures 2a and 2d**). Compared with the 834 cm^{-1} absorption in 1.4m LiFSI Py13FSI+TTE, the addition of TTE and FDG does not cause any noticeable absorption shift. However, introducing DG enables an absorption shift closer to the Py13FSI absorption (without LiFSI) at 828.5 cm^{-1}, which suggests a strong solvation of Li$^+$ by DG (**Figure 2e**) that increases the portion of non-solvated FSI anions.

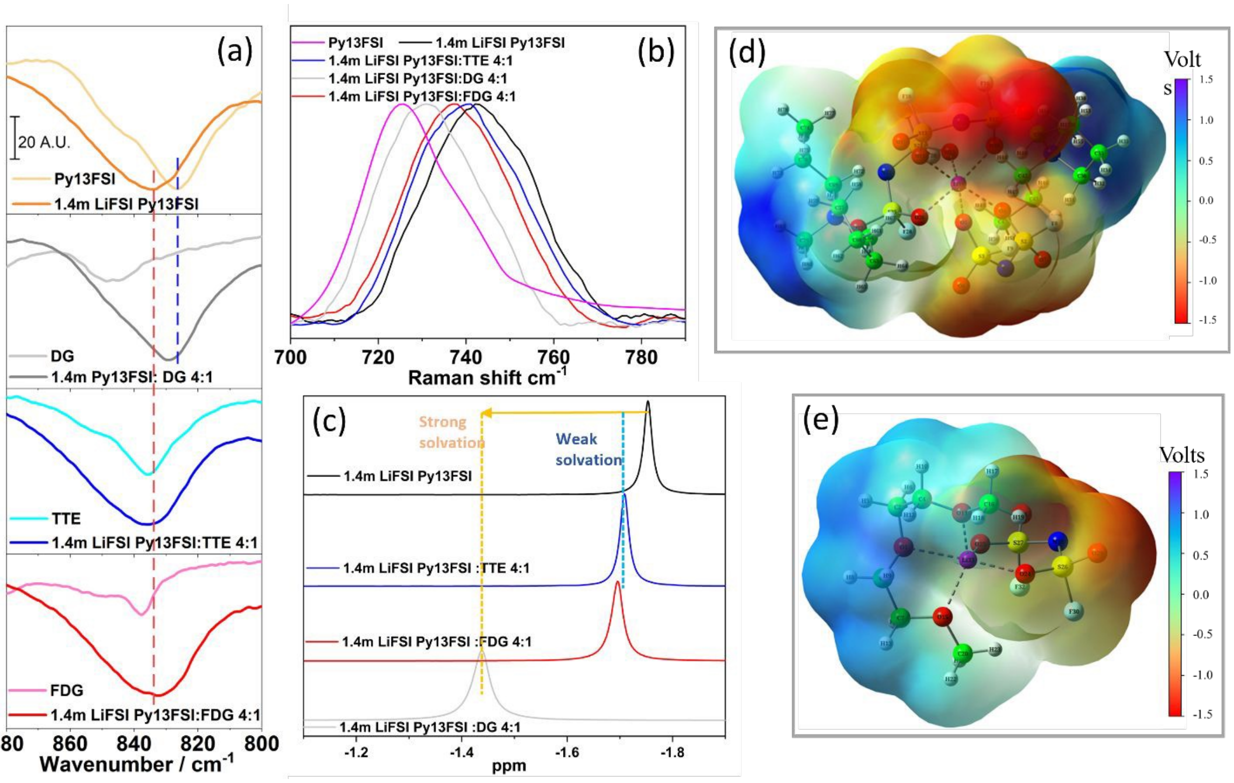

Figure 2. (a) FTIR spectra for the four electrolytes in the wavenumber range of showing S-N-S asymmetric stretching from the FSI anion; Absorption of cosolvents at the same range were plotted to show their noninterference of the S-N-S signal in the electrolyte; (b) ^{7}Li NMR spectra for the four electrolytes revealing the chemical environment of Li$^+$ in the solvation sheath; (c) Raman spectra for the four electrolytes probing S-N-S asymmetric stretching from the FSI anion; Ab initio optimized structures of a cluster depicting (d) the coordination between DG/FSI$^-$ and Li$^+$ and corresponding MEP surface, and (e) coordination between FSI$^-$ and Li$^+$ and corresponding MEP.

To further investigate the solvation capabilities of the different cosolvents, especially FDG and TTE, we conducted Raman spectroscopy focusing on the sulfonyl vibration (700-780 cm^{-1}) in the four electrolytes

DOI: 10.1039/D5EE01515D

(**Figure 2b**). There is a 17 cm^{-1} absorption shift from the IL (725 cm^{-1}) to Py13FSI electrolyte with 1.4m LiFSI (742 cm^{-1}) due to the Li^+ coordination by the FSI anion. Similar to the IR data, adding DG leads to an absorption shift to lower wavenumbers at about 730 cm^{-1}, (i.e. closer to Py13FSI without lithium salt) indicating a strong solvation capability of DG (**Figure 2e**) that reduces the coordination ratio between FSI and Li^+. In contrast, the minimal shift towards lower wavenumbers (737 cm^{-1} and 740 cm^{-1}) relative to 1.4m LiFSI Py13FSI at 740 cm^{-1} caused by FDG and TTE reveals their moderate solvation capabilities. The relatively smaller shift of TTE suggests its lower solvation power compared to FDG. Please note that the non-solvating nature of TTE has been reported in localized high concentration electrolytes as a diluent.[3, 20] To further verify the solvation capabilities of the cosolvents, we probed the chemical environment of Li^+ ions through ^{7}Li NMR spectroscopy. The coordination between DG and Li^+ significantly shifts the ^{7}Li signal to high field, as observed in **Figure 2c**, whereas low-solvating-power TTE and FDG as cosolvents, which exert weak interaction with Li^+, exhibit less shift of the ^{7}Li signal. Less shift stemming from FDG than TTE also indicates FDG's higher solvation power than TTE, which is in good agreement with the Raman data. Strong solvation exerted by DG would increase its population in the inner solvation sheath surrounding Li^+ that will bring in significant DG-electrolyte features (i.e. poor cycling stability in LMBs) over the relatively stable cycling feature of the neat IL-based electrolyte.

To gain further insights into the solvation structures, classic molecular dynamic (MD) simulations were carried out to picturize the solvation structures of these IL-based electrolytes. The snapshots in **Figures 3a, 3b and 3c** demonstrate that Li^+ closely interacts with FSI^- clouds in the solvation sheath whereas positioning $Py13^+$ cations at the peripheral distance. The introduction of cosolvents (blue clouds) affects the solvation sheath to different extents due to their varied electronic and solvating properties. Radial distribution functions (RDF, **Figure 3d**) reveal the distribution of several ion pairs between Li cations and FSI anions and oxygens from cosolvents. RDF of Li-O_{FSI} (**Figure S3**) shows modest difference in the inner shell (2.0-2.4 Å) of all four electrolytes due to the relatively low concentration of LiFSI salt and low volumetric percentage (20%) of the cosolvents. The saturation number of five at the 2-3 Å range observed in the

View Article Online
DOI: 10.1039/D5EE01515D

cumulative number analysis (**Figure 3f**) indicates a coordination number of five, which is mostly between Li^+ and FSI^-, in all targeted electrolytes. From the cosolvent aspect; however, RDF of Li-O_{DG}, Li-O_{TTE}, and Li-O_{FDG} exhibits noticeable differences in the medial range of 3.0-6.0 Å. The two broad peaks centered at 3.5 and 5.3 Å in Li-O_{DG} spectrum manifests that DG forms two shells outside the inner sheath constituted by Li^+ and FSI^-due to its strong solvation capability. In contrast, FDG and TTE exhibit weaker solvation power as indicated by their RDF peaks at a farther distance of 5~6 Å. Ab initio calculation results in **Figures 3g and 3h** depict relative positioning of Li^+, FSI^-, and cosolvents (i.e. Li^+ and cosolvents do not show direct coordination). The lower onset of Li-O_{FDG} RDF peak than that of Li-O_{TTE} verifies the weaker solvation power of TTE, which agrees well with the Raman and NMR results. The cumulative distribution of cosolvents (**Figure 3e**) further confirms the order of solvation power (DG > FDG > TTE) by the descending population from DG, FDG, to TTE in the radial range of 4-6 Å. Our solvation study along with electrochemical results showed evidence that the solvation differences across these four electrolytes exert significant influence on lithium plating/stripping and interphase formation, which will be covered in sections below.

View Article Online
DOI: 10.1039/D5EE01515D

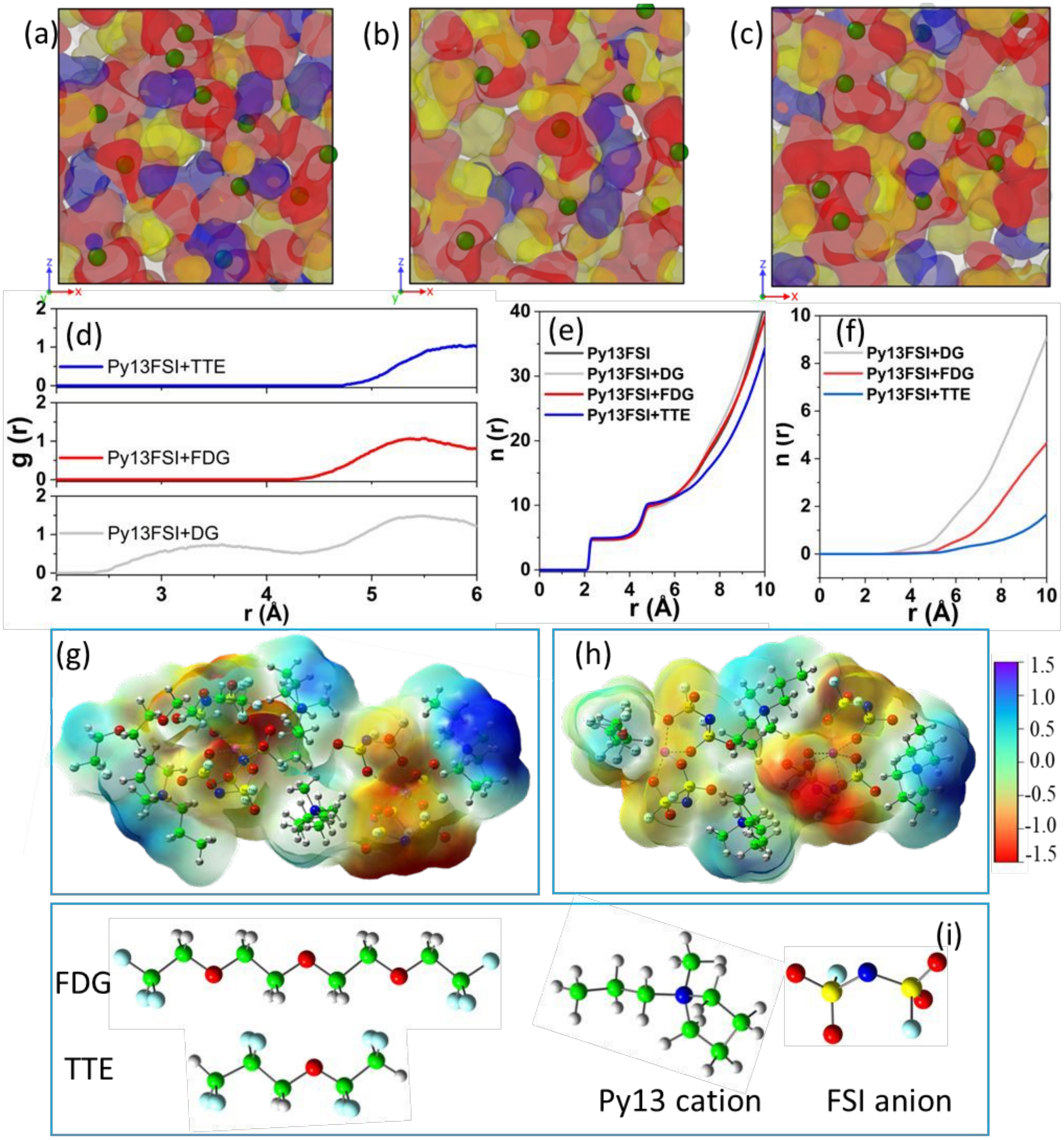

Figure 3. MD simulation boxes output for (a) Py13FSI+DG electrolyte, (b) Py13FSI+FDG electrolyte, (c) Py13FSI+TTE electrolyte. Green spheres, red, yellow, and blue clouds stand for Li ions, FSI anions, Py13 cations, and cosolvents. Plots of (d) radial distribution functions of Li-O$_{cosolv}$, (e) cumulative number analysis of Li-O$_{FSI}$, for electrolytes mixed with different cosolvents. (f) cumulative number analysis of Li-O$_{cosolv}$, Ab initio optimized structures showing their sheaths MEP (color scales in volts) of (g) a cluster constructed with four Py13FSI, two LiFSI, and one FDG molecules depicting the typical solvation sheath

View Article Online
DOI: 10.1039/D5EE01515D

structure of the Py13FSI+FDG electrolyte, and (h) a cluster constructed with three Py13FSI, two LiFSI, and one TTE molecules, standing for Py13FSI+TTE electrolyte. (i) ball-stick model of molecular structures used in the ab initio optimization All simulations are based on the formulation 1.4m LiFSI in Py13FSI:cosolvent (4:1 v/v)

Facilitating lithium plating/stripping with FDG cosolvent: Given the distinct solvation capabilities enabled by different cosolvents, our next goal is to evaluate the lithium plating/stripping efficiency in these IL-based electrolytes. We first monitored the time-lapsed voltage profiles in symmetric Li||Li cells when applying a current density of 1 mA cm^{-2}. It is evident that Py13FSI and Py13FSI+DG display significant polarization, whereas TTE and FDG are beneficial to stabilize Li cycling, as evidenced by the lower and more stable polarization (**Figure 4d**). The efficiency of the Li plating/stripping process was also assessed through measuring the coulombic efficiency (CE) of Li||Cu cells (**Figures 4a, 4b and 4c**). The Li||Cu cells employing the different electrolytes were operated using the Aurbach protocol.[36, 37] A reservoir lithium layer with a capacity of 4 mAh cm^{-2} was deposited onto a copper foil at a current density of 0.1 mAcm^{-2}. Following this, plating and stripping processes were conducted at a current density of 1 mA cm^{-2} for nine cycles. Subsequently, all the lithium was stripped at 0.1 mAcm^{-2} until the cell potential reached 1.0 V. The Py13FSI+FDG cell demonstrates the highest CE of 98.9% among the Li||Cu cells using three different electrolytes, where the other two cells show lower CEs of 96.4% and 97.8% using Py13FSI and Py13FSI+TTE, respectively. The Py13FSI+DG electrolyte is not able to complete the protocol in Li||Cu cells due to severe side reactions. The results of the Li||Cu cell tests agree well with the galvanostatic cycling results, revealing that Py13FSI+FDG outperforms the other three electrolytes, showing suppressed side reactions as evidenced by the higher CE. The Py13FSI+TTE and Py13FSI+FDG cells outperform the neat Py13FSI cell in terms of CE, which is possibly due to the reduced viscosity upon mixing with cosolvents as diluents. Despite the lower viscosity in Py13FSI+TTE, its lower CE than Py13FSI+FDG could stem from the more significant aluminum corrosion as evidenced by the higher leakage current shown in potentiostatic hold experiments (**Figure S4**). From the aspect of lithium-ion transport, although the addition

View Article Online
DOI: 10.1039/D5EE01515D

of cosolvents reduces the overall conductivities (**Figures S5 and S6**) of the electrolytes since Py13FSI itself is conductive, the Py13FSI+FDG electrolyte exhibits a lithium transference number (t^{+}_{Li}) of 0.73, which is significantly higher than that of the Py13FSI electrolyte ($t^{+}_{Li} = 0.53$) (**Figure S7**). The enhanced Li transport in the Py13FSI+FDG electrolyte could be one of the reasons for the more efficient lithium plating/stripping, and thus the better cycling performance (*vide infra*). The significant increase in the transference number of the Py13FSI+FDG electrolyte could stem from the moderate solvating capability (i.e. mostly through the centered oxygen with higher electron density than the two terminal oxygens adjacent to trifluoromethyl groups) that can perturbate the Li-FSI interactions (i.e. much more FSI anions exist than Li ions in this case) and enable more free Li ions as mobile charge carriers. This can, in contrast, corroborate with the addition of TTE cosolvent that does not lead to a significant difference in transference numbers due to its non-solvating nature. Note that the unchanged transference number with DG as cosolvent may be because of the much stronger lithium solvation capability of DG than Py13FSI, which enables it to be the primary coordinating solvent for the LiFSI salt. As a result of that, the ionic liquid no longer functions as a weakly coordinating medium forming Li^{+}–FSI^{-} clusters, but instead acts as a weakly solvating background solvent.

View Article Online
DOI: 10.1039/D5EE01515D

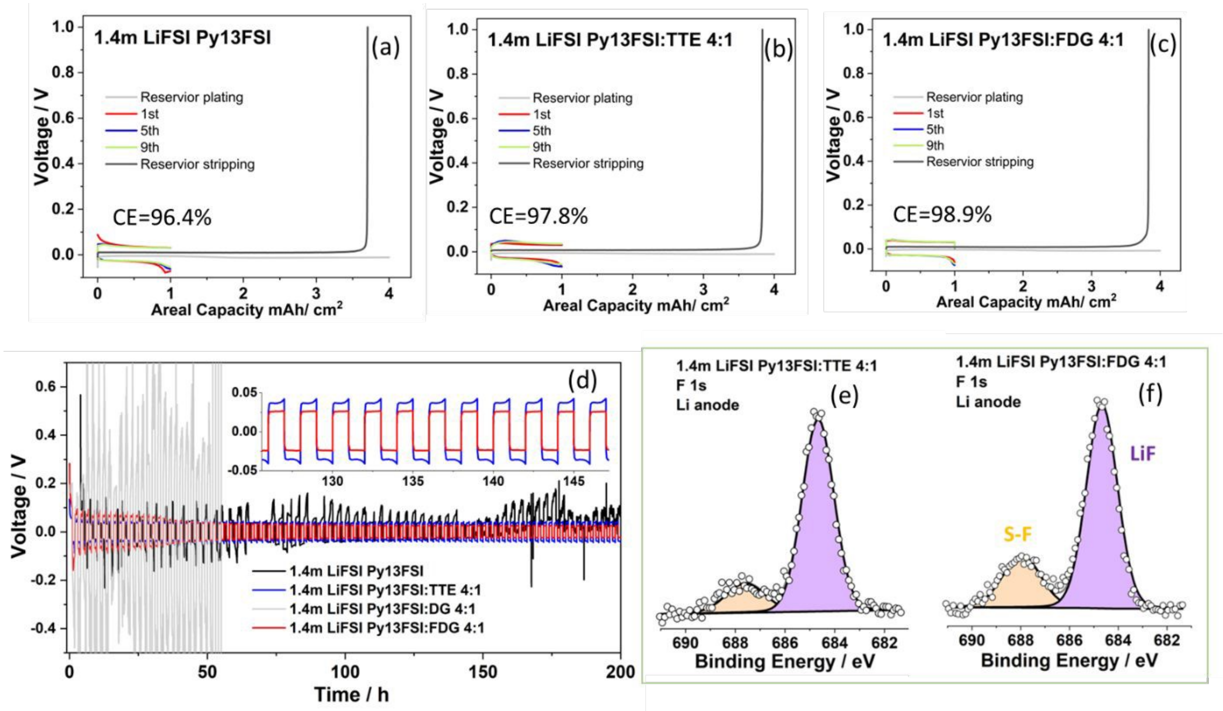

Figure 4. Voltage profiles of Li||Cu cells for selected cycles that contain the different electrolytes studied herein, i.e., (a) Py13FSI, (b) Py13FSI+TTE, (c) Py13FSI+FDG. All Li||Cu cells were cycled according to the Auerbach protocol. (d) Voltage profiles of Li||Li symmetrical cells with targeted electrolytes; F1s XPS spectra from the Li anode cycled in (e) Py13FSI+TTE (f) Py13FSI+FDG electrolytes in Li||NMC cells.

FDG Enabled Stable Cycling of Li||NMC811 Cells Using Py13FSI-based Electrolyte: The evaluation of electrochemical stabilities of the four electrolytes was carried out in cells with an NMC 811 cathode and Li anode. The cells were cycled at C/2 after three formation cycles at C/10 with the cut-off voltages being 3.0 and 4.3 V (**Figure 5a**). Among these formulations, Py13FSI+FDG demonstrated a persistently stable capacity throughout the first 200 cycles and a notable improvement in capacity retention of 95% (156 mAh g^{-1}) at 250 cycles, compared to the pristine Py13FSI electrolyte (14%, 25 mAh g^{-1}). The cell using the Py13FSI electrolyte without any cosolvent remains stable for only 50 cycles, and shows a rapid capacity decay beginning after 50 cycles. Following FDG, the addition of TTE as cosolvent was investigated, which exhibits an enhanced capacity retention of 83 mAh g^{-1} after 250 cycles. However, prior to the continuous capacity drop after 75 cycles, a noticeable first-stage capacity decay from 184 to 162 mAh g^{-1} appeared from 40 to 75 cycle, which is close to the decaying point of the Py13FSI cell. Therefore, the similar starting

DOI: 10.1039/D5EE01515D

point of capacity decay between Py13FSI and Py13FSI+TTE cells indicates that using TTE as cosolvent does not sufficiently stabilize the Li||NMC811 cell to avoid the first-stage capacity decay (40-75 cycle), although it can still alleviate the rapid capacity drop after 75 cycles, which is observed in the Py13FSI cell. In contrast to the other three formulations, the introduction of DG results in a rapid capacity dip starting already from the 2nd cycle, indicating low stability and severe side reactions of the electrolyte.

Analyzing selected voltage profiles after various cycles offers deeper insights into the evolving electrochemical behavior of the electrolytes over the course of cycling. As shown in **Figures 5b, 5c,5d and S3**, the four electrolytes provide a first-cycle discharge capacity of 183, 189, 181, and 157 mAh g^{-1} for Py13FSI, Py13FSI+TTE, Py13FSI+FDG, and Py13FSI+DG cells, respectively. The first-cycle discharge capacity of the Py13FSI+TTE cell, recorded at 189 mAh g^{-1}, outperforms the other electrolytes, but shows significant capacity fading after 100 cycles, with a capacity of 118 mAh g^{-1} after 200 cycles (**Figure 5c**). In comparison, Py13FSI exhibits quicker apparent capacity depletion at earlier cycles than Py13FSI+TTE. Despite slightly lower first-cycle capacity, the overall capacity retention of Py13FSI+FDG outperforms the other formulations, providing a specific capacity of 166 mAh g^{-1} (92% of peak discharge capacity) after 200 cycles (**Figure 5d**). The deviation of the voltage profiles from the original in formulations other than Py13FSI+FDG signifies deteriorating cycling stability of the IL-based electrolytes without an appropriate cosolvent.

The Coulombic efficiency (CE) (**Figure 5a**) of the Li||NMC811 cells reflects the reversibility of the lithium plating/stripping process in the designated electrolyte environments, as irreversibility is primarily attributed to the electrochemical stabilities of electrolytes against lithium metal anode.[38, 39] As summarized in **Table S1**, the average CE in the first 200 cycles of the three cells using Py13FSI, Py13FSI+TTE, and Py13FSI+FDG is 99.15%, 99.79%, and 99.74%, respectively. The leakage current of Li||NMC cells collected from potentiostatic hold experiments (**Figure S8**) also confirmed that FDG cosolvent did not compromise the anodic stability at voltages up to 4.6V, despite its oxidative potential is relatively lower than that of TTE. Besides the highest average CE, Py13FSI+FDG also shows the most stable cycling

View Article Online
DOI: 10.1039/D5EE01515D

without noticeable decay or deviation points in CE like its counterparts do (**Figure 5a**). Such observation indicates the enhanced electrolyte stability and reversibility of the Li plating/stripping process enabled by the incorporation of FDG as cosolvent. However, please also note that in the current electrolyte system, increasing volumetric ratio of FDG did not further extend the cycling life of Li||NMC cell (**Figure S9**), possibly due to the higher extent of side reactions from the decomposition of Li-FDG clusters. The low cosolvent ratio also guarantees the non-flammability nature of Py13FSI is well retained in the electrolyte solution, which has been proved by the ignition tests shown in **Figure S10**.

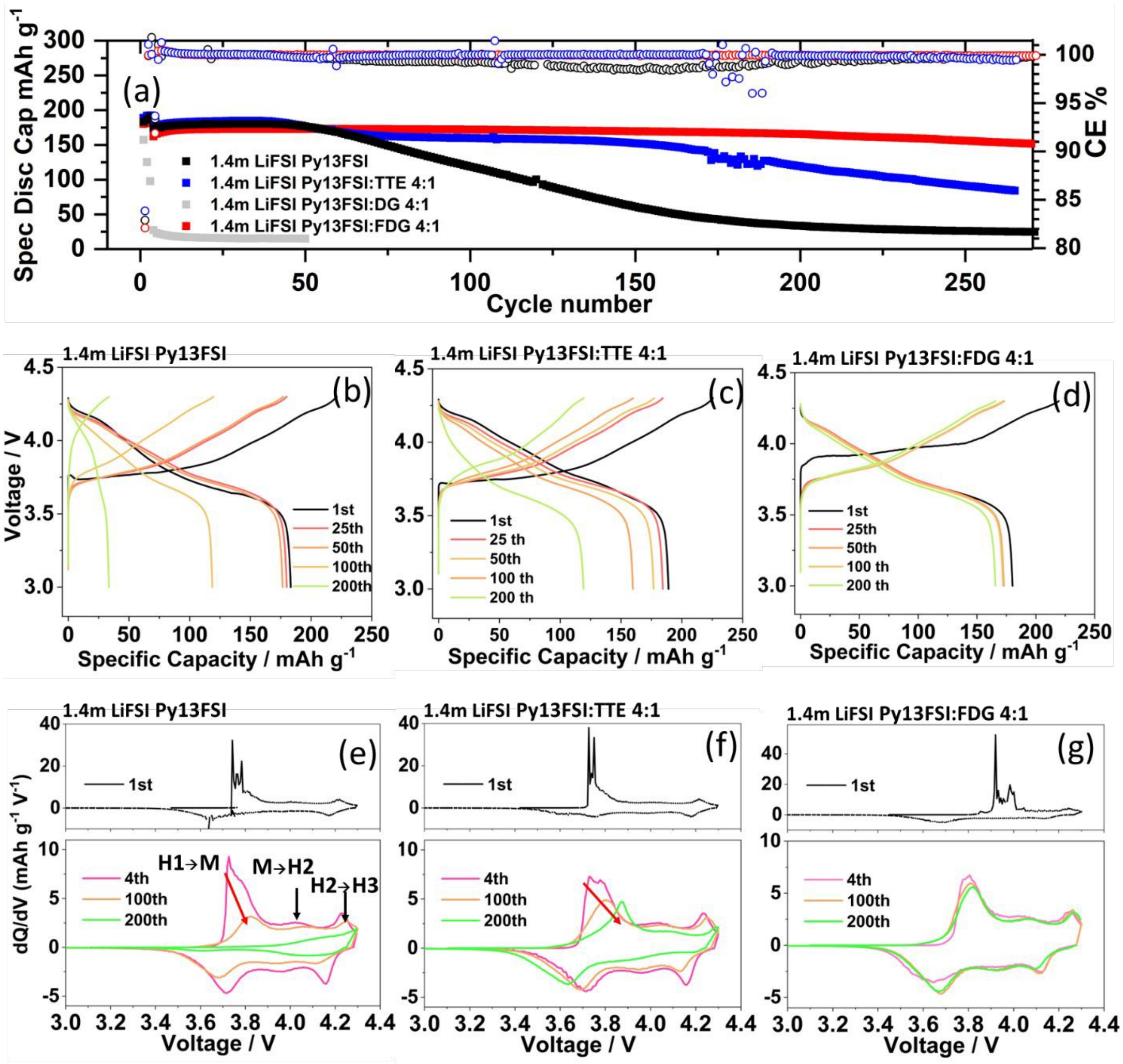

View Article Online
DOI: 10.1039/D5EE01515D

Figure 5. (a) Evolution of discharge capacity and CE of Li||NMC811 cells containing different electrolytes. The cells were cycled at C/3 with cut-off voltages of 3.0 and 4.3 V; (b)-(d) Selected voltage-capacity curves of Li||NMC811 cells with different electrolytes at certain cycles; (e) Voltage profiles of symmetric Li||Li cells with different electrolytes. Differential capacity curves at selected cycles in Li||NMC811 cells containing (d) Py13FSI, (e) Py13FSI+TTE, and (f) Py13FSI+FDG as the electrolyte.

Robust cathode-electrolyte interphase initiated by FDG cosolvent: To gain insights into the electrochemical processes occurring between the electrolytes and NMC811, we examined the differential capacity (dQ/dV) plots displayed in **Figures 5e, 5f and 5g**. NMC811 cathode features three characteristic redox peaks at about 3.7, 4.0, and 4.2 V, assigned to the Li intercalation process in three stages: phase transition from a hexagonal (H1) to monoclinic (M) lattice, M to hexagonal (H2), and H2 to hexagonal (H3).[40-42] For both Py13FSI and Py13FSI+TTE, the differential capacity plots (**Figures 5e and 5f**) of the first cycle (i.e. a formation cycle at C/10) do not show significant potential difference in contrast to the fourth cycle (*i.e.* the first cycle at C/3). However, the NMC811 cathode in Py13FSI+FDG cell displays an overpotential of 0.1 V compared with the fourth cycle (i.e., 3.9 V in the 1st cycle and 3.8 V for the 4th cycle), which suggests the formation of a passivation layer on the cathode with this electrolyte. The prompt alleviation of overpotential since 2nd cycle (**Figure S11**) indicates that the build of desired interphase facilities lithium intercalation and deintercalation in the cathode. This can be further confirmed by the XPS results (Figure 6) that shows the distinct CEI components of the FDG electrolyte from the other three electrolytes. With the poorest cycling results, the Py13FSI+DG cell (**Figure S12**) shows obvious polarization in the third cycle and crowded spikes for the fourth, indicating severe side reactions and degradation of the electrolyte.

Compared with the initial cycles, a dramatic diminishing of the H1→M peak and an overpotential of 0.1 V (3.7 to 3.8 V) are observed after 100 cycles in the Li||NMC811 cell using Py13FSI electrolyte, where the H2→H3 peaks are attenuated as well. As cycling progresses to 200 cycles, the redox features related to the H1→M and M→H2 transitions completely vanished, and a further faded H2→H3 signal with a higher overpotential of 0.2 V is observed. The shift and attenuation of the signature phase-transition signals

View Article Online
DOI: 10.1039/D5EE01515D

indicate a pronounced irreversibility of these reactions in these cells.[43] In contrast, the H1→M phase transition of the cell employing Py13FSI+TTE as the electrolyte after 200 cycles shows a comparable intensity to the 100th cycle, although a higher overpotential at 3.9 V is still observed. The M→H2 phase intensity is mostly retained at 200 cycles whereas the H2→H3 phase decayed significantly, which is similar to the Py13FSI cell. With the best capacity retention in this work, the Py13FSI+FDG cell retains all three phase-transformation signals intact without noticeable overpotential and intensity decay (**Figure 5g**). Since the XRD patterns collected from the cycled cathodes confirmed the intact nature of the NMC materials in all electrolytes (**Figure S13**), the overpotential built during cycling is attributed to detrimental interphases formed between the cathode and the given electrolytes. As seen in **Figure 5f**, the remaining transition signals related to the H1→M and M→H2 transitions (compare with Py13FSI electrolyte in **Figure 5e**) suggest that TTE as a cosolvent is helpful to stabilize the Li^+ intercalation during such phase transition to some extent. In the Py13FSI+FDG case, the overpotential-free characteristic even at 200 cycles verifies that the interphase in this case is robust and favorable for the Li^+ cation transport.[44] Unlike the other three cells capable of cycling over 100 times, the instability of Py13FSI+DG electrolyte is also reflected in the dQ/dV curve (**Figure S14**), which shows the loss of all phase-transition peaks at the 4th cycle. This could stem from the strong solvation of DG with Li^+, resulting in the solvation sheath not favorable for the formation of robust interphases, which will be further discussed in the solvation section.

To probe the formation of interphases as a function of electrolyte formulations, we collected electrochemical impedance spectroscopy (EIS) data of Li||NMC cells after formation cycles to monitor the impedance of interphases. The EIS data (**Figure S15a**) in the frequency range from 500 kHz to 120 Hz (i.e. the first arch in the Nyquist plot in this work) reflects the resistance of the interphase film at the surface of electrodes.[24] As shown in the spectra, the Li||NMC cell with Py13FSI+FDG as the electrolyte shows the lowest interphase resistance among the three tested electrolytes, whereas the absence of any cosolvent in the Py13FSI electrolyte results in the largest interphase resistance. The progressive establishment of the interphase between the electrolytes and electrodes during repeated Li^+ de-/intercalation using the different

View Article Online
DOI: 10.1039/D5EE01515D

electrolytes can cause distinct charge-transfer kinetics that will further affect the long-term electrochemical performance of the cells.[43, 45] Note that the EIS measurements in this work do not distinguish detailed interfacial electrochemistry occurring on the cathode and anode interfaces individually. However, the EIS measured in symmetric Li||Li cells (**Figure S15b**) after 15 cycles at 1mA cm^{-2} displayed similar interphase resistances (reflected by the first arch in the Nyquist plot) on the Li surface across the three electrolytes, which suggests similar properties of the interphases formed on the Li surface. This observation corroborates the XPS results for the SEI in presence of the different electrolytes (*vide infra*). Therefore, we attribute such interfacial-resistance difference observed in Li||NMC cells to different cathode interphase formation caused by varying the cosolvent. The cathode interphase with a low resistance established in Py13FSI+FDG favors lithium transport as cycling progressed, which aligns with the stable overpotential at high cycle numbers in **Figure 3f**.

Distinct solvation structures, by influencing the species distribution within the inner or secondary sheath, may lead to different interfacial processes occurring between the electrolyte components and electrodes (i.e. either cathode, anode or both). We thus studied the surface chemistry of the electrodes after cycling by X-ray photoelectron spectroscopy (XPS) (**Figure 4e, 4f, Figure 6, and Table S2**). On the lithium anode surface (**Figure 4e, 4f**), two major components, SO_2-F and LiF at 687.5 and 684.5 eV, respectively, were identified from the deconvoluted F1s spectra collected from cells with Py13FSI and Py13FSI+FDG. The SO_2-F and LiF species suggest that the SEI is mainly formed from the decomposition of FSI anions in both electrolytes. The addition of 20% (volume) FDG does not result in significant changes of the anode-surface components other than a slight increase of the SO_2-F content (i.e. 24.2% in Py13FSI+FDG cells) compared to Py13FSI+TTE (16.3%) and Py13FSI (22.5%) (**Figures 4e, 4f, S16, and Table S2**). Note that no noticeable C-F species from the decomposition of FDG or TTE were identified on the anode surface. The similar XPS profiles collected from the anodes for all three electrolytes indicates moderate changes of the SEI when adding the cosolvents, which is in good agreement with the EIS results collected from Li||Li cells after cycling at 1 mA cm^{-2} for 15 cycles, where similar interphase (SEI)

View Article Online
DOI: 10.1039/D5EE01515D

resistances were observed for all three cases (**Figure S15b**). The moderate changes in SEI species among the three electrolytes are due to the high concentration (relatively higher than commonly used 1M LiFSI) of FSI anions that are more favorable to decompose to form a stable SEI than the ethereal cosolvents, which corroborates with the two identified species (**Figure 4e, 4f**) signaturing FSI decomposition.[17, 20] On the cathode side, however, the addition of FDG leads to an interphase containing noticeably more SO_2-F from FSI decomposition, as observed in the F1s spectra in **Figure 6**, compared to Py13FSI and Py13FSI+TTE. Furthermore, the C1s spectra on the cathode retrieved from cells with Py13FSI+FDG as the electrolyte reveal 6% of CF_3 species (291 eV, **Figure 6d**) that are supposed to be generated from oxidative degradation of FDG.[46] Differently, CF_2 species at 290 eV [43] from TTE decomposition were not apparent on the cathode, evidenced by a similar C-F content in the F1s and C1s XPS spectra (**Figures 6a and 6b**) compared to Py13FSI (**Figure S16**). These findings are intriguing since MD simulations revealed negligible differences on the FSI quantities within the inner solvation sheath (2.0-2.4 Å), whereas the introduction of cosolvents apparently alters the interfacial chemistry through FSI degradation at the cathode surface. We reckon that the properties of shell in the medial range to Li^+ (4-10 Å) where nearest cosolvent molecules reside in, determined by solvation capabilities of cosolvents, could be critical for such different surface behaviors on the cathode. Taking these observations together, the arising of more organic species (SO_2-F and C-F) from decomposition of FDG and FSI- in Py13FSI+FDG electrolyte is crucial for the stabilization of the cathode-electrolyte interphase. Such interphase with optimal physical and electrochemical properties can facilitate lithium intercalations with suppressed overpotential (**Figures 4a, 4b and 4c**) and side reactions.

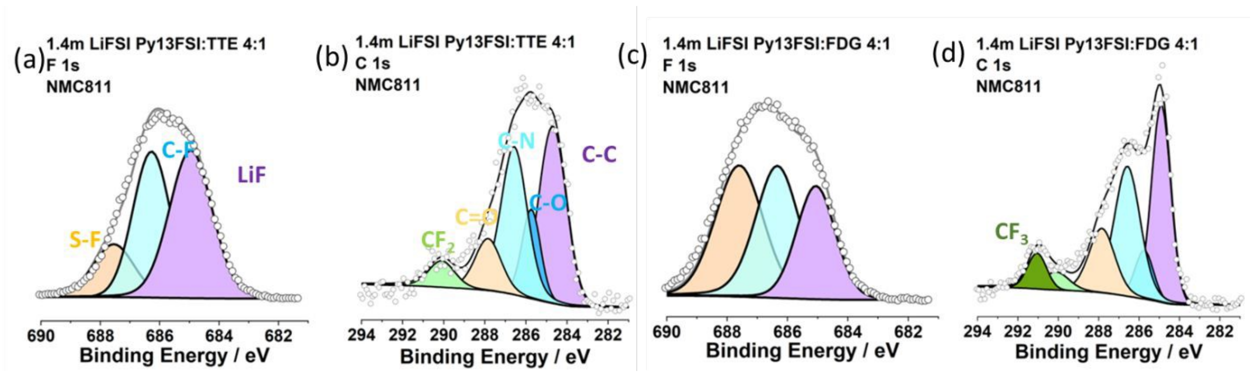

View Article Online
DOI: 10.1039/D5EE01515D

Figure 6. Deconvoluted XPS results collected from NMC811 cathode dissembled from cells filled with Py13FSI+FDG and Py13FSI+TTE electrolyte after cycling tests. (a) F1s and (b) C1s spectra from the NMC cathode cycled in Py13FSI+TTE electrolyte. (c) F1s and (d) C1s spectra from the NMC811 cathode cycled in Py13FSI+FDG electrolyte.

Conclusion

In this study, we found that FDG, when used as a cosolvent in ionic-liquid-based electrolytes, significantly extends the cycling life of the Py13FSI electrolyte. Electrochemical and surface analyses confirm that this improvement results from the formation of a favorable cathode interphase, which enables an efficient Li^+ transport with reduced over potential. Spectroscopic techniques, including FTIR, Raman, and NMR, as well as MD simulations, reveal the different solvation structures in Py13FSI-based electrolytes when adding cosolvents with varying solvation abilities. The mild solvating strength and lithium stability of FDG are key factors behind its success. In contrast, DG, a strong solvating solvent, dramatically alters the solvation shell of the ionic liquid electrolyte, making the Py13FSI-DG electrolyte unstable at the lithium metal anode. On the other hand, TTE, which is a non-solvating solvent, fails to enhance the lithium transport in the Py13FSI-TTE electrolyte and does not form a stable interphase on the cathode surface. Thus, FDG, with its balanced solvating properties, provides the optimal solution. Our comparisons with TTE and DG show that a medium-range solvation shell is crucial for facilitating the formation of a stable electrolyte-cathode interphase, potentially through FSI decomposition. This work will guide the future development of long-lasting ionic liquid-based electrolytes.

ASSOCIATED CONTENT

Supporting Information

This material is available free of charge via the Internet.

AUTHOR INFORMATION

Corresponding Author

View Article Online
DOI: 10.1039/D5EE01515D

*Email: csu@anl.gov; seminario@tamu.edu; balbuena@tamu.edu; amine@anl.gov

Notes

The authors declare no competing financial interest.

ACKNOWLEDGMENTS

This work was conducted as part of the U.S.-German joint collaboration on "Interfaces and Interphases in Rechargeable Li-metal Based Batteries" supported by the U.S. Department of Energy (DOE) and the German Federal Ministry of Education and Research (BMBF). Financial support was provided by the U.S. Department of Energy (DOE), Vehicle Technologies Office (VTO). Argonne National Laboratory is operated for the DOE Office of Science by UChicago Argonne, LLC, under contract number DE-AC02-06CH11357 under the U.S.-Germany Cooperation on Energy Storage. The NMC electrodes were manufactured at the DOE's CAMP Facility, at Argonne National Laboratory. The CAMP Facility is fully supported by the DOE VTO within the core funding of the Applied Battery Research for Transportation Program. P.B.B. and J.M.S. acknowledge DOE through the US–Germany Cooperation on Energy Storage under Contract DE-AC02-05CH11357. Z.L. and D.B. acknowledge the financial support from the Helmholtz Association and the BMBF within the LILLINT-2 project (03XP0511E). Computational resources from the Texas A&M University High Performance Research Computing are gratefully acknowledged.

KEYWORDS

Lithium metal batteries, fluorinated glycol ether, optimal solvating cosolvent, ionic liquid electrolyte, electrolyte solvation.

Reference

View Article Online
DOI: 10.1039/D5EE01515D

(1) Cheng, X.-B.; Zhang, R.; Zhao, C.-Z.; Zhang, Q. Toward Safe Lithium Metal Anode in Rechargeable Batteries: A Review. *Chemical Reviews* **2017**, *117* (15), 10403-10473. DOI: 10.1021/acs.chemrev.7b00115.
(2) Lin, D.; Liu, Y.; Cui, Y. Reviving the lithium metal anode for high-energy batteries. *Nature Nanotechnology* **2017**, *12* (3), 194-206. DOI: 10.1038/nnano.2017.16.
(3) Ren, X.; Zou, L.; Cao, X.; Engelhard, M. H.; Liu, W.; Burton, S. D.; Lee, H.; Niu, C.; Matthews, B. E.; Zhu, Z.; et al. Enabling High-Voltage Lithium-Metal Batteries under Practical Conditions. *Joule* **2019**, *3* (7), 1662-1676. DOI: https://doi.org/10.1016/j.joule.2019.05.006.
(4) Zhao, Y.; Zhou, T.; Ashirov, T.; Kazzi, M. E.; Cancellieri, C.; Jeurgens, L. P. H.; Choi, J. W.; Coskun, A. Fluorinated ether electrolyte with controlled solvation structure for high voltage lithium metal batteries. *Nature Communications* **2022**, *13* (1), 2575. DOI: 10.1038/s41467-022-29199-3.
(5) Yu, Z.; Wang, H.; Kong, X.; Huang, W.; Tsao, Y.; Mackanic, D. G.; Wang, K.; Wang, X.; Huang, W.; Choudhury, S.; et al. Molecular design for electrolyte solvents enabling energy-dense and long-cycling lithium metal batteries. *Nature Energy* **2020**, *5* (7), 526-533. DOI: 10.1038/s41560-020-0634-5.
(6) Zhao, W.; Zheng, J.; Zou, L.; Jia, H.; Liu, B.; Wang, H.; Engelhard, M. H.; Wang, C.; Xu, W.; Yang, Y.; et al. High Voltage Operation of Ni-Rich NMC Cathodes Enabled by Stable Electrode/Electrolyte Interphases. *Advanced Energy Materials* **2018**, *8* (19), 1800297. DOI: https://doi.org/10.1002/aenm.201800297 (acccessed 2024/04/29).
(7) Zhang, Z.; Yang, J.; Huang, W.; Wang, H.; Zhou, W.; Li, Y.; Li, Y.; Xu, J.; Huang, W.; Chiu, W.; et al. Cathode-Electrolyte Interphase in Lithium Batteries Revealed by Cryogenic Electron Microscopy. *Matter* **2021**, *4* (1), 302-312. DOI: https://doi.org/10.1016/j.matt.2020.10.021.
(8) Heist, A.; Hafner, S.; Lee, S.-H. High-Energy Nickel-Rich Layered Cathode Stabilized by Ionic Liquid Electrolyte. *Journal of The Electrochemical Society* **2019**, *166* (6), A873. DOI: 10.1149/2.0071906jes.
(9) Wu, H.; Jia, H.; Wang, C.; Zhang, J.-G.; Xu, W. Recent Progress in Understanding Solid Electrolyte Interphase on Lithium Metal Anodes. *Advanced Energy Materials* **2021**, *11* (5), 2003092. DOI: https://doi.org/10.1002/aenm.202003092 (acccessed 2024/04/29).
(10) Cheng, X.-B.; Zhang, R.; Zhao, C.-Z.; Wei, F.; Zhang, J.-G.; Zhang, Q. A Review of Solid Electrolyte Interphases on Lithium Metal Anode. *Advanced Science* **2016**, *3* (3), 1500213. DOI: https://doi.org/10.1002/advs.201500213 (acccessed 2024/04/29).
(11) Fan, X.; Wang, C. High-voltage liquid electrolytes for Li batteries: progress and perspectives. *Chemical Society Reviews* **2021**, *50* (18), 10486-10566, 10.1039/D1CS00450F. DOI: 10.1039/D1CS00450F.
(12) Wang, Y.; Li, Z.; Hou, Y.; Hao, Z.; Zhang, Q.; Ni, Y.; Lu, Y.; Yan, Z.; Zhang, K.; Zhao, Q.; et al. Emerging electrolytes with fluorinated solvents for rechargeable lithium-based batteries. *Chemical Society Reviews* **2023**, *52* (8), 2713-2763, 10.1039/D2CS00873D. DOI: 10.1039/D2CS00873D.
(13) Ren, X.; Zou, L.; Jiao, S.; Mei, D.; Engelhard, M. H.; Li, Q.; Lee, H.; Niu, C.; Adams, B. D.; Wang, C.; et al. High-Concentration Ether Electrolytes for Stable High-Voltage Lithium Metal Batteries. *ACS Energy Letters* **2019**, *4* (4), 896-902. DOI: 10.1021/acsenergylett.9b00381.
(14) Alvarado, J.; Schroeder, M. A.; Pollard, T. P.; Wang, X.; Lee, J. Z.; Zhang, M.; Wynn, T.; Ding, M.; Borodin, O.; Meng, Y. S.; et al. Bisalt ether electrolytes: a pathway towards lithium metal batteries with Ni-rich cathodes. *Energy & Environmental Science* **2019**, *12* (2), 780-794, 10.1039/C8EE02601G. DOI: 10.1039/C8EE02601G.
(15) Camacho-Forero, L. E.; Smith, T. W.; Balbuena, P. B. Effects of High and Low Salt Concentration in Electrolytes at Lithium–Metal Anode Surfaces. *The Journal of Physical Chemistry C* **2017**, *121* (1), 182-194. DOI: 10.1021/acs.jpcc.6b10774.
(16) Jiao, S.; Ren, X.; Cao, R.; Engelhard, M. H.; Liu, Y.; Hu, D.; Mei, D.; Zheng, J.; Zhao, W.; Li, Q.; et al. Stable cycling of high-voltage lithium metal batteries in ether electrolytes. *Nature Energy* **2018**, *3* (9), 739-746. DOI: 10.1038/s41560-018-0199-8.

View Article Online
DOI: 10.1039/D5EE01515D

(17) Chen, S.; Zheng, J.; Mei, D.; Han, K. S.; Engelhard, M. H.; Zhao, W.; Xu, W.; Liu, J.; Zhang, J.-G. High-Voltage Lithium-Metal Batteries Enabled by Localized High-Concentration Electrolytes. *Advanced Materials* **2018**, *30* (21), 1706102. DOI: https://doi.org/10.1002/adma.201706102 (acccessed 2023/08/14).

(18) Ren, X.; Chen, S.; Lee, H.; Mei, D.; Engelhard, M. H.; Burton, S. D.; Zhao, W.; Zheng, J.; Li, Q.; Ding, M. S.; et al. Localized High-Concentration Sulfone Electrolytes for High-Efficiency Lithium-Metal Batteries. *Chem* **2018**, *4* (8), 1877-1892. DOI: https://doi.org/10.1016/j.chempr.2018.05.002.

(19) Perez Beltran, S.; Cao, X.; Zhang, J.-G.; Balbuena, P. B. Localized High Concentration Electrolytes for High Voltage Lithium–Metal Batteries: Correlation between the Electrolyte Composition and Its Reductive/Oxidative Stability. *Chemistry of Materials* **2020**, *32* (14), 5973-5984. DOI: 10.1021/acs.chemmater.0c00987.

(20) Cao, X.; Jia, H.; Xu, W.; Zhang, J.-G. Review—Localized High-Concentration Electrolytes for Lithium Batteries. *Journal of The Electrochemical Society* **2021**, *168* (1), 010522. DOI: 10.1149/1945-7111/abd60e.

(21) Karimi, N.; Zarrabeitia, M.; Mariani, A.; Gatti, D.; Varzi, A.; Passerini, S. Nonfluorinated Ionic Liquid Electrolytes for Lithium Metal Batteries: Ionic Conduction, Electrochemistry, and Interphase Formation. *Advanced Energy Materials* **2021**, *11* (4), 2003521. DOI: https://doi.org/10.1002/aenm.202003521 (acccessed 2024/04/29).

(22) Wang, Z.; Zhang, F.; Sun, Y.; Zheng, L.; Shen, Y.; Fu, D.; Li, W.; Pan, A.; Wang, L.; Xu, J.; et al. Intrinsically Nonflammable Ionic Liquid-Based Localized Highly Concentrated Electrolytes Enable High-Performance Li-Metal Batteries. *Advanced Energy Materials* **2021**, *11* (17), 2003752. DOI: https://doi.org/10.1002/aenm.202003752 (acccessed 2024/04/29).

(23) Sun, H.; Zhu, G.; Zhu, Y.; Lin, M.-C.; Chen, H.; Li, Y.-Y.; Hung, W. H.; Zhou, B.; Wang, X.; Bai, Y.; et al. High-Safety and High-Energy-Density Lithium Metal Batteries in a Novel Ionic-Liquid Electrolyte. *Advanced Materials* **2020**, *32* (26), 2001741. DOI: https://doi.org/10.1002/adma.202001741 (acccessed 2024/04/29).

(24) Liu, Q.; Jiang, W.; Xu, J.; Xu, Y.; Yang, Z.; Yoo, D.-J.; Pupek, K. Z.; Wang, C.; Liu, C.; Xu, K.; et al. A fluorinated cation introduces new interphasial chemistries to enable high-voltage lithium metal batteries. *Nature Communications* **2023**, *14* (1), 3678. DOI: 10.1038/s41467-023-38229-7.

(25) Yoo, D.-J.; Kim, K. J.; Choi, J. W. The Synergistic Effect of Cation and Anion of an Ionic Liquid Additive for Lithium Metal Anodes. *Advanced Energy Materials* **2018**, *8* (11), 1702744. DOI: https://doi.org/10.1002/aenm.201702744 (acccessed 2024/04/29).

(26) Hasanpoor, M.; Eftekharnia, M.; Pathirana, T.; Pal, U.; Kerr, R.; Forsyth, M.; Howlett, P. C. Understanding the Role of Separator and Electrolyte Compatibility on Lithium Metal Anode Performance Using Ionic Liquid-Based Electrolytes. *ACS Applied Energy Materials* **2021**, *4* (6), 6310-6323. DOI: 10.1021/acsaem.1c01114.

(27) Zhou, Q.; Henderson, W. A.; Appetecchi, G. B.; Montanino, M.; Passerini, S. Physical and Electrochemical Properties of N-Alkyl-N-methylpyrrolidinium Bis(fluorosulfonyl)imide Ionic Liquids: PY13FSI and PY14FSI. *The Journal of Physical Chemistry B* **2008**, *112* (43), 13577-13580. DOI: 10.1021/jp805419f.

(28) Ong, S. P.; Andreussi, O.; Wu, Y.; Marzari, N.; Ceder, G. Electrochemical Windows of Room-Temperature Ionic Liquids from Molecular Dynamics and Density Functional Theory Calculations. *Chemistry of Materials* **2011**, *23* (11), 2979-2986. DOI: 10.1021/cm200679y.

(29) Liu, X.; Mariani, A.; Diemant, T.; Pietro, M. E. D.; Dong, X.; Kuenzel, M.; Mele, A.; Passerini, S. Difluorobenzene-Based Locally Concentrated Ionic Liquid Electrolyte Enabling Stable Cycling of Lithium Metal Batteries with Nickel-Rich Cathode. *Advanced Energy Materials* **2022**, *12* (25), 2200862. DOI: https://doi.org/10.1002/aenm.202200862 (acccessed 2024/04/29).

View Article Online
DOI: 10.1039/D5EE01515D

(30) Lee, S.; Park, K.; Koo, B.; Park, C.; Jang, M.; Lee, H.; Lee, H. Safe, Stable Cycling of Lithium Metal Batteries with Low-Viscosity, Fire-Retardant Locally Concentrated Ionic Liquid Electrolytes. *Advanced Functional Materials* **2020**, *30* (35), 2003132. DOI: https://doi.org/10.1002/adfm.202003132 (acccessed 2024/04/29).
(31) Liu, X.; Mariani, A.; Diemant, T.; Dong, X.; Su, P.-H.; Passerini, S. Locally Concentrated Ionic Liquid Electrolytes Enabling Low-Temperature Lithium Metal Batteries. *Angewandte Chemie International Edition* **2023**, *62* (31), e202305840. DOI: https://doi.org/10.1002/anie.202305840 (acccessed 2024/04/29).
(32) Borodin, O.; Gorecki, W.; Smith, G. D.; Armand, M. Molecular Dynamics Simulation and Pulsed-Field Gradient NMR Studies of Bis(fluorosulfonyl)imide (FSI) and Bis[(trifluoromethyl)sulfonyl]imide (TFSI)-Based Ionic Liquids. *The Journal of Physical Chemistry B* **2010**, *114* (20), 6786-6798. DOI: 10.1021/jp911950q.
(33) Yoon, H.; Best, A. S.; Forsyth, M.; MacFarlane, D. R.; Howlett, P. C. Physical properties of high Li-ion content N-propyl-N-methylpyrrolidinium bis(fluorosulfonyl)imide based ionic liquid electrolytes. *Physical Chemistry Chemical Physics* **2015**, *17* (6), 4656-4663, 10.1039/C4CP05333H. DOI: 10.1039/C4CP05333H.
(34) Wang, Z.; Zhang, H.; Han, R.; Xu, J.; Pan, A.; Zhang, F.; Huang, D.; Wei, Y.; Wang, L.; Song, H.; et al. Establish an Advanced Electrolyte/Graphite Interphase by an Ionic Liquid-Based Localized Highly Concentrated Electrolyte for Low-Temperature and Rapid-Charging Li-Ion Batteries. *ACS Sustainable Chemistry & Engineering* **2022**, *10* (36), 12023-12029. DOI: 10.1021/acssuschemeng.2c03938.
(35) Tu, H.; Li, L.; Wang, Z.; Wang, J.; Lin, H.; Wang, M.; Yan, C.; Liu, M. Tailoring Electrolyte Solvation for LiF-Rich Solid Electrolyte Interphase toward a Stable Li Anode. *ACS Nano* **2022**, *16* (10), 16898-16908. DOI: 10.1021/acsnano.2c06924.
(36) Li, X.; Wu, X.; Doan, H. A.; Yang, Z.; Amine, R.; Li, M.; Bracamonte, M. V.; Su, C.-C.; Amine, K. Acidity-Governed Rules in the Electrochemical Performance of Fluorinated Benzenes for High-Voltage Lithium Metal Batteries. *ACS Energy Letters* **2024**, *9* (7), 3484-3491. DOI: 10.1021/acsenergylett.4c01215.
(37) Adams, B. D.; Zheng, J.; Ren, X.; Xu, W.; Zhang, J.-G. Accurate Determination of Coulombic Efficiency for Lithium Metal Anodes and Lithium Metal Batteries. *Advanced Energy Materials* **2018**, *8* (7), 1702097. DOI: https://doi.org/10.1002/aenm.201702097 (acccessed 2024/04/30).
(38) Ko, S.; Obukata, T.; Shimada, T.; Takenaka, N.; Nakayama, M.; Yamada, A.; Yamada, Y. Electrode potential influences the reversibility of lithium-metal anodes. *Nature Energy* **2022**, *7* (12), 1217-1224. DOI: 10.1038/s41560-022-01144-0.
(39) Liu, H.; Cheng, X.-B.; Xu, R.; Zhang, X.-Q.; Yan, C.; Huang, J.-Q.; Zhang, Q. Plating/Stripping Behavior of Actual Lithium Metal Anode. *Advanced Energy Materials* **2019**, *9* (44), 1902254. DOI: https://doi.org/10.1002/aenm.201902254 (acccessed 2025/01/16).
(40) Zheng, S.; Hong, C.; Guan, X.; Xiang, Y.; Liu, X.; Xu, G.-L.; Liu, R.; Zhong, G.; Zheng, F.; Li, Y.; et al. Correlation between long range and local structural changes in Ni-rich layered materials during charge and discharge process. *Journal of Power Sources* **2019**, *412*, 336-343. DOI: https://doi.org/10.1016/j.jpowsour.2018.11.053.
(41) Jung, R.; Metzger, M.; Maglia, F.; Stinner, C.; Gasteiger, H. A. Oxygen Release and Its Effect on the Cycling Stability of LiNixMnyCozO2 (NMC) Cathode Materials for Li-Ion Batteries. *Journal of The Electrochemical Society* **2017**, *164* (7), A1361. DOI: 10.1149/2.0021707jes.
(42) de Biasi, L.; Schiele, A.; Roca-Ayats, M.; Garcia, G.; Brezesinski, T.; Hartmann, P.; Janek, J. Phase Transformation Behavior and Stability of LiNiO2 Cathode Material for Li-Ion Batteries Obtained from In Situ Gas Analysis and Operando X-Ray Diffraction. *ChemSusChem* **2019**, *12* (10), 2240-2250. DOI: https://doi.org/10.1002/cssc.201900032 (acccessed 2024/04/30).
(43) Wu, F.; Fang, S.; Kuenzel, M.; Mullaliu, A.; Kim, J.-K.; Gao, X.; Diemant, T.; Kim, G.-T.; Passerini, S. Dual-anion ionic liquid electrolyte enables stable Ni-rich cathodes in lithium-metal batteries. *Joule* **2021**, *5* (8), 2177-2194. DOI: https://doi.org/10.1016/j.joule.2021.06.014.

View Article Online
DOI: 10.1039/D5EE01515D

(44) Kim, J.-H.; Kim, S. J.; Yuk, T.; Kim, J.; Yoon, C. S.; Sun, Y.-K. Variation of Electronic Conductivity within Secondary Particles Revealing a Capacity-Fading Mechanism of Layered Ni-Rich Cathode. *ACS Energy Letters* **2018**, *3* (12), 3002-3007. DOI: 10.1021/acsenergylett.8b02043.
(45) Rao, Y.; Li, X.; Zhao, S.; Liu, P.; Wu, F.; Liu, X.; Zhou, N.; Fang, S.; Passerini, S. Fluorinated electrolyte formulations design enabling high-voltage and long-life lithium metal batteries. *Nano Energy* **2024**, *123*, 109362. DOI: https://doi.org/10.1016/j.nanoen.2024.109362.
(46) Liu, Q.; Xu, J.; Jiang, W.; Gim, J.; Tornheim, A. P.; Pathak, R.; Zhu, Q.; Zuo, P.; Yang, Z.; Pupek, K. Z.; et al. High-Energy LiNiO2 Li Metal Batteries Enabled by Hybrid Electrolyte Consisting of Ionic Liquid and Weakly Solvating Fluorinated Ether. *Advanced Science* **2024**, *11* (46), 2409662. DOI: https://doi.org/10.1002/advs.202409662 (acccessed 2025/01/14).

View Article Online
DOI: 10.1039/D5EE01515D

Data Availability Statement

The data that support the findings of this study are available from the corresponding author upon reasonable request.